JGR Oceans

RESEARCH ARTICLE
10.1029/2021JC017458

Key Points:

- In the tropical Northwest Pacific, DOM dynamics was jointly regulated by physical processes, phytoplankton production, photochemical reactions and microbial processes
- In the tropical Northwest Pacific, organic matter fluorescence effectively traces frontal mixing processes
- The quasi-permanent cold Mindanao and warm Halmahera eddy pair enhanced lateral dissolved organic matter transport in the western boundary current system

Supporting Information:

Supporting Information may be found in the online version of this article.

Correspondence to:

W. Guo,
wdguo@xmu.edu.cn

Citation:

Wang, C., Li, Y., Li, Y., Zhou, H., Stubbins, A., Dahlgren, R. A., et al. (2021). Dissolved organic matter dynamics in the epipelagic Northwest Pacific low-latitude western boundary current system: Insights from optical analyses. *Journal of Geophysical Research: Oceans*, *126*, e2021JC017458. https://doi.org/10.1029/2021JC017458

Received 12 APR 2021
Accepted 12 AUG 2021

Dissolved Organic Matter Dynamics in the Epipelagic Northwest Pacific Low-Latitude Western Boundary Current System: Insights From Optical Analyses

Chao Wang[1,2], Yizhen Li[3,4], Yan Li[2], Hui Zhou[5], Aron Stubbins[6], Randy A. Dahlgren[7], Zhiheng Wang[1,2], and Weidong Guo[1,2]

[1]State Key Laboratory of Marine Environmental Science, College of Ocean and Earth Sciences, Xiamen University, Xiamen, China, [2]Fujian Provincial Key Laboratory for Coastal Ecology and Environmental Studies, Xiamen University, Xiamen, China, [3]CSS Inc. Under Contract to National Centers for Coastal Ocean Science, National Oceanic and Atmospheric Administration, Silver Spring, MD, USA, [4]Department of Applied Ocean Physics and Engineering, Woods Hole Oceanographic Institution, Woods Hole, MA, USA, [5]Key Laboratory of Ocean Circulation and Waves, Institute of Oceanography, Chinese Academy of Sciences, Qingdao, China, [6]Departments of Marine and Environmental Sciences, Civil and Environmental Engineering, and Chemistry and Chemical Biology, Northeastern University, Boston, MA, USA, [7]Department of Land, Air, and Water Resources, University of California Davis, Davis, CA, USA

Abstract High-resolution horizontal and vertical distribution of dissolved organic carbon (DOC), chromophoric, and fluorescent dissolved organic matter (CDOM and FDOM) were investigated in the western boundary current system of the tropical Northwest Pacific (<200 m) in autumn 2017. A strong correlation between DOC and stratification index indicated that the vertical DOC profile was primarily regulated by physical processes. The association of high $a_{CDOM}(254)$ with the maximum chlorophyll (Chl *a*) layer infers phytoplankton-sourced dissolved organic matter (DOM). The $a_{CDOM}(325)$ and humic-like FDOM ($FDOM_H$) showed an accumulation in the deeper layer and positive correlations with apparent oxygen utilization and Chl *a* concentration at the maximum chlorophyll layer, suggesting that these components are related to microbial degradation of biogenic materials. Elevated Chl *a* at the frontal area between the North Equatorial Current (NEC) and cold Mindanao Eddy enhanced DOM production. Input waters from the NEC showed higher DOC, but lower $FDOM_H$, than inflow waters from the New Guinea Coastal Current/Undercurrent (NGC(U)C). A mass balance model estimated a 6-times higher lateral DOC flux from the NEC tropical-gyre branch (12°N–7.5°N) than that from the subtropical-gyre branch (12°N–17°N). Based on comparison with long-term (1994–2015) average DOC fluxes for the same season, eddy and upstream processes contributed 38%, 46% and 40% of lateral DOC fluxes for the NEC tropical-gyre branch, NGC(U)C and export North Equatorial Counter Current, respectively. These results demonstrated that the quasi-permanent Mindanao and Halmahera eddies greatly enhance lateral export of DOM with altered properties throughout this large conjunction area.

Plain Language Summary The tropical Northwest Pacific Ocean is a crossroads linking large-scale water transport among the North, South and central Pacific, and tropical Indian Ocean. Hydrological processes within this area are very dynamic due to mixing of multiple water currents and the occurrence of mesoscale cold and warm eddies. In this study, we assessed how these complex hydrological processes regulate the quality and quantity of dissolved organic matter (DOM) based on high-resolution horizontal and vertical investigations of DOM optical properties. The mixed layer depth largely regulated the vertical patterns for dissolved organic carbon and DOM optical properties. Notably, elevated chlorophyll-*a* concentrations associated with mixing dynamics at the frontal area increased DOM production. A mass balance model using field current velocity data revealed that dynamic eddy processes greatly enhanced lateral export of DOM. This work highlights the importance of lateral and vertical hydrodynamic processes in controlling carbon biogeochemistry of the surface ocean.

1. Introduction

Dissolved organic matter (DOM) is the largest reduced carbon (C) pool in the global ocean, with a dissolved organic carbon (DOC) inventory (662 ± 32 Gt) similar to that of the atmospheric CO_2 pool (Hansell et al., 2009). Previous basin-scale studies found distinctive horizontal and vertical variations in epipelagic

DOM quantity and quality among different biogeographic provinces (Catalá et al., 2016; Iuculano et al., 2019; Kowalczuk et al., 2013). Various biological (planktonic population and productivity), chemical (nutrient level, apparent oxygen utilization [AOU]), and photochemical factors were posited to regulate the production-degradation dynamics of the epipelagic DOM pool (Catalá et al., 2016; Mopper et al., 2015; Rochelle-Newall & Fisher, 2002). Hydrodynamic processes, such as lateral, vertical (e.g., mesoscale eddies) and frontal mixing between different currents, may further modulate epipelagic DOM quantity/composition through regulation of the aforementioned biogeochemical factors (Wang et al., 2017; Wu et al., 2015). However, owing to the lack of data with high spatial resolution, the combined hydrological and biogeochemical regulation of oceanic DOM cycling remains poorly understood.

The tropical Northwest Pacific Ocean encompasses complex current structures, which form the low-latitude western boundary current system (Hu et al., 2015). As a crossroad linking large-scale water transport among the North, South and central Pacific, and tropical Indian Ocean (~150 Sv, 1 Sv = 10^6 m^3 s^{-1}) (Qu et al., 1998), the tropical Northwest Pacific is a dynamic area with considerable lateral transport and exchange of DOM with the global open ocean (Wang, 2019; Wijffels et al., 2008). In addition, the confluence of different water currents in this region propagates the quasi-persistent cold Mindanao Eddy and warm Halmahera Eddy (Kashino et al., 2013; Zhou et al., 2010). This mesoscale eddy pair could affect surface DOM dynamics and its vertical transport by generating the upwelling and subduction of water masses, thereby influencing nutrient supply, primary production, and microbial DOM production/degradation (Jiao et al., 2014; Moutin & Prieur, 2012; Wang et al., 2017). Seasonal and interannual variations of the Mindanao and Halmahera eddy pair could regulate the lateral DOM flux through modulating fluctuations in lateral transport volumes of the associated currents (Kashino et al., 2013). Thus, the tropical Northwest Pacific is an ideal laboratory for studying the hydrodynamic regulation of oceanic DOM transformation and transport dynamics.

Optical analyses of DOM (i.e., absorption and fluorescence) are widely applied to characterize the sources and transformation/transport dynamics of chromophoric DOM (CDOM) and fluorescent DOM (FDOM) in the global ocean (Jørgensen et al., 2011; Nelson et al., 2010; Yamashita et al., 2017). Absorption coefficients at different wavelengths (e.g., 254, 325, 350, and 443 nm) and fluorescence intensities at selected excitation/emission wavelength pairs are commonly used as quantitative indicators of DOM components (e.g., humic-like peaks C and M [$FDOM_H$] and protein-like peaks T and B) (Coble, 1996; Guo et al., 2007; Qu et al., 2020). Similarly, the spectral slope ($S_{275-295}$), carbon-normalized absorbance (e.g., $SUVA_{325}$) and fluorescence indices (e.g., HIX) are widely used as qualitative proxies (Hansen et al., 2016; Helms et al., 2008; Ohno, 2002). Ultraviolet A and visible chromophore levels (e.g., $a_{CDOM}(325)$) and $FDOM_H$ generally increase with depth in the open ocean (Jørgensen et al., 2011; Nelson et al., 2010), decrease during photo irradiation (Helms et al., 2013), and increase during microbial dark incubation (Rochelle-Newall & Fisher, 2002). This implies that these DOM fractions accumulate in the aphotic ocean and are photo-labile and bio-refractory. Levels of ultraviolet C chromophores (e.g., $a_{CDOM}[254]$) and protein-like FDOM (peak T) are largest in the euphotic ocean and decrease both with depth and during microbial dark incubation (Cai et al., 2019; Shen & Benner, 2019). This infers that these components are depleted in the dark ocean and are photo-refractory and bio-labile. Thus, optical analyses can provide valuable information regarding the quantity, quality, and biogeochemical reactivity of DOM.

In this study, high-resolution horizontal and vertical investigations of epipelagic (depth <200 m) DOC, CDOM and FDOM were conducted in autumn 2017 along two orthometric transects in the tropical Northwest Pacific, which captures three different currents and two quasi-persistent mesoscale eddies. Combined with hydrographical, nutrient, oxygen, and chlorophyll *a* (Chl *a*) data, the physical and biogeochemical drivers shaping the three-dimensional fine structure of DOM parameters were elucidated. Lateral DOC transport fluxes in this region were estimated using a simplified mass balance model, including the unobserved Indonesian Throughflow. Comparison of model-simulated average velocity during the cruise period to the long-term (1994–2015) climatic velocity data allowed us to evaluate the role of Mindanao and Halmahera eddy pair activities on DOM lateral transport.

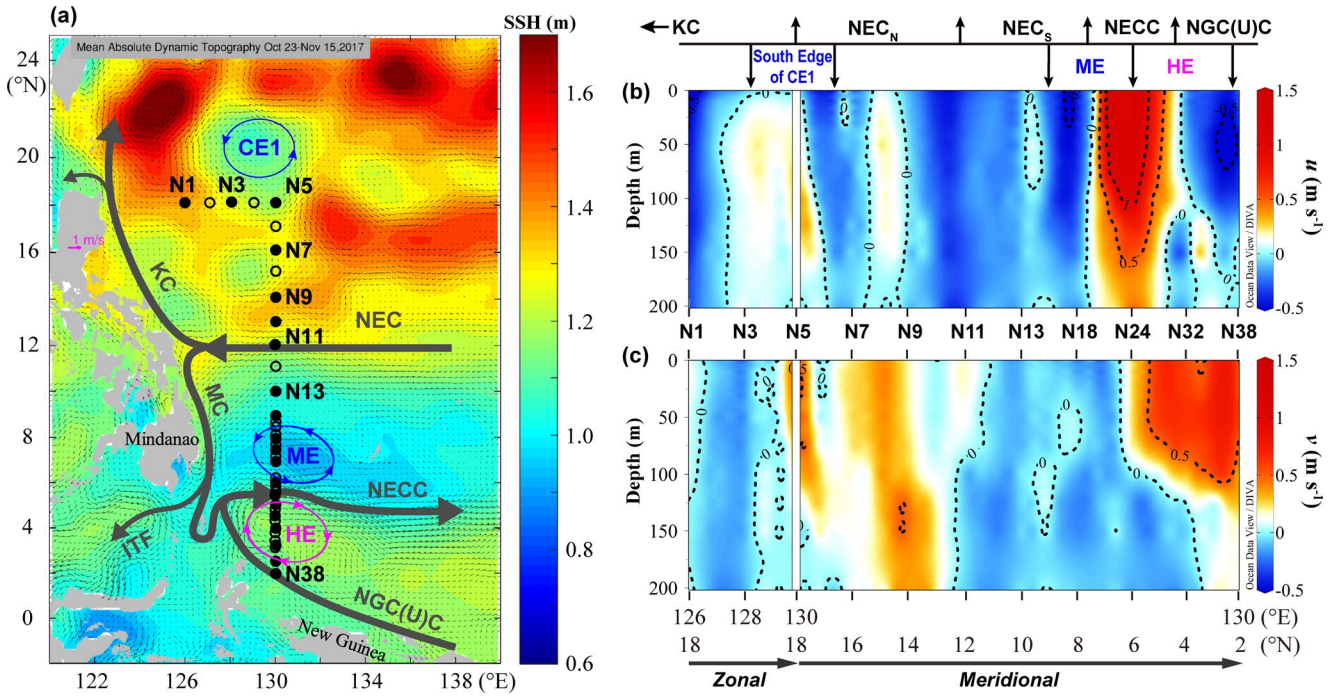

Figure 1. (a) Schematic of major currents and observation stations in the tropical Northwest Pacific Ocean during the cruise period (October–November 2017). The background is the sea surface height (SSH, colored) and the surface geostrophic currents (vectors) from AVISO data. NEC, North Equatorial Current; KC, Kuroshio Current; MC, Mindanao Current; NECC, North Equatorial Counter Current; ITF, Indonesian Throughflow; NGC(U)C, New Guinea Coastal Current and Undercurrent. The Mindanao Eddy (ME) and cyclonic eddy 1 (CE1) are highlighted as blue circles, and the Halmahera Eddy (HE) is highlighted as a red circle. All 38 stations are hydrographic stations, among which the 20 solid circles represent stations for biogeochemical sampling. (b and c) The variabilities of simulated zonal velocity (u) and meridional velocity (v) in the upper 200 m along the zonal 18°N and meridional 130°E transects from HYCOM data. Positive u and v values represent currents flowing from west to east and from south to north, respectively. Stations are divided into three currents (North Equatorial Current, North Equatorial Countercurrent, and New Guinea Coastal Current and Undercurrent) and three eddies (ME, HE, and ACE1) and are labeled at the top of subpanel (b).

2. Materials and Methods

2.1. Study Area

Two input currents and three export currents comprise the epipelagic tropical Northwest Pacific (Figure 1a) (Hu et al., 2015). The North Equatorial Current (NEC) flows westward from the central to western Pacific. Upon approaching the Philippine coast, the NEC splits into the poleward Kuroshio Current and the equatorward Mindanao Current. Part of the Mindanao Current converges with the northwestward-flowing New Guinea Coastal Current and Undercurrent (NGC(U)C) from the South Pacific, retroflecting to support the eastward-flowing North Equatorial Countercurrent (NECC) back to the central Pacific (Donguy & Meyers, 1996; Ueki et al., 2003). The other part of the Mindanao Current flows into the Celebes Sea feeding the main branch of the Indonesian Throughflow (Gordon & Fine, 1996; Wijffels et al., 2008). Due to their large variability and strong interactions, these currents enhance mesoscale activities in this region (Qiu & Chen, 2010; Zhou et al., 2021). In particular, the interactions of the Mindanao Current and NGC(U)C at their retroflection points generate the quasi-persistent cold Mindanao Eddy and warm Halmahera eddy pair (Arruda & Nof, 2003).

2.2. Identification of Currents and Mesoscale Eddies During the Cruise Period

Field observations were conducted onboard the R/V *KEXUE* from October 25 to November 12, 2017 along the meridional 130°E transect (2°N–18°N) and a shorter zonal 18°N transect (126°E–130°E) in the tropical Northwest Pacific (Figure 1a). Since the synoptic current field derived from the cruise is a little noisy, we obtained sea surface height and corresponding surface geostrophic current data from Archiving, Validation, and Interpretation of Satellite Oceanographic data (AVISO) (Figure 1a) and simulated velocities

from the Hybrid Coordinate Ocean Model (HYCOM) (Figures 1b and 1c) to identify the range of currents and mesoscale eddies during the cruise period. Along the 130°E transect, the northwestward NGC(U)C (2°N–4°N) and the northern subtropical-gyre branch (12°N–17°N) of NEC (NEC_N) showed negative zonal (i.e., westward) and positive meridional (i.e., northward) velocities. In contrast, the southern tropical-gyre branch (12°N–7.5°N) of NEC (NEC_S), a transitional frontal area of the NEC with the Mindanao Eddy, had negative zonal (i.e., westward) and meridional (i.e., southward) velocities. The eastward NECC (7.5°N–4°N) had a positive zonal velocity. The zonal 18°N transect showed low southward velocity thus not covering the main branch of the northward Kuroshio Current. The quasi-permanent Mindanao (centered at 7.5°N) and Halmahera (centered at 4°N) eddies covered about 3°. Stations N4 and N5 were located at the south edge of a transient cold eddy (CE1) centered at ~20°N, 128°E. Okubo-Weiss values indicated that these eddies were stable and relatively active during the cruise period (Figure S1).

2.3. Field Observations, Data Acquisition, and Sampling

High resolution lateral observations at 0.25° intervals were conducted south of 8°N along the 130°E transect where the water currents showed large variations (Hu et al., 2015); the interval was 1° for the other stations. Profiles of temperature, salinity, dissolved oxygen (DO), and Chl *a* fluorescence were obtained at 38 hydrographic stations (black dots and circles in Figure 1a) in the upper 200-m water column using a calibrated SBE 911plus CTD unit, fitted with a Chl *a* fluorometer (WETLab, USA) and dissolved oxygen sensor (SeaBird SBE43). The conductivity, temperature and pressure sensors were calibrated in the laboratory before the cruise. The factory-supplied Scale Factor (WETlab, USA) was used to calibrate the Chl *a* fluorescence intensity (RFU) determined by an *in situ* fluorometer as Chl *a* ($\mu g\ L^{-1}$). Chl *a* concentrations of 20 discrete samples were determined by a Turner Trilogy fluorometer (Welschmeyer, 1994). Linear regression analysis of fluorescence versus extractable Chl *a* generated a slope of 1.12 ± 0.06, hence the factory-supplied Scale Factor was deemed appropriate. Oxygen sensor calibration was carried out with 176 discrete samples measured on board with the Winkler titration method (Carpenter, 1965). Dissolved oxygen saturation was calculated from the salinity and potential temperature with the equation of Benson and Krause (1984). Apparent oxygen utilization (AOU) was calculated as the difference between the calculated saturation and measured dissolved oxygen concentrations.

The depth of the mixed layer was calculated as the depth where the potential density exceeded the value at 1 m by 0.1 kg m^{-3} (Liu et al., 2017). The squared Brunt-Väisälä frequency (N^2) is commonly used to quantify the degree of water column stratification (Catalá et al., 2016; Lønborg et al., 2015). Higher N^2 values indicate stronger stratification. Following Millard et al. (1990), N^2 was calculated as:

$$N^2 = -\frac{g}{\rho}\cdot\frac{\partial\rho}{\partial z} = -g\cdot\frac{\partial \ln(\rho)}{\partial z}, \quad (1)$$

where g is the gravity acceleration constant (9.8 m s^{-2}), z is the water depth, and ρ is the water density at depth z. Integration of Equation 1 between two depth levels (z_1 and z_2): $\overline{N}^2 = -g\ln(\rho_2/\rho_1)/(z_2-z_1)$, provides an average stability of the epipelagic tropical Northwest Pacific between 3 m (z_1) and 200 m (z_2).

Water samples for inorganic nutrients (nitrate, nitrite, and phosphate), DOC, CDOM, and FDOM were collected at 20 biogeochemical stations (black dots in Figure 1a). Typically, seven to nine depths were sampled at 18 stations with a 24 (10 L) Niskin bottles rosette. High-resolution vertical sampling was conducted at station N27 (5.25°N, 130°E) and N35 (3.25°N, 130°E) at 5–10 m intervals in the upper 200 m. Samples for inorganic nutrient analyses were filtered through MF-Millipore™ filters (0.45 μm) and stored frozen until analysis. Samples for DOC, CDOM and FDOM analyses were filtered immediately through pre-combusted (500°C, 5 h) GF/F filters (nominal pore size ~0.7 μm) into pre-combusted glass vials with Teflon-lined caps under a gentle vacuum of <150 mm Hg (Catalá et al., 2018; Martínez-Pérez et al., 2019; Yamashita et al., 2017). DOC samples were acidified with H_3PO_4 (85%, Merck) to pH < 2 and stored frozen until analysis. CDOM and FDOM samples were stored in the dark at 4°C until analysis within 1 month after the cruise (Spencer & Coble, 2014).

2.4. Inorganic Nutrients and DOC Analyses

Inorganic nutrients were analyzed onboard using a four-channel continuous flow Technicon AA3 Auto-Analyzer (Bran-Lube GmbH). Detection limits for nitrate plus nitrite (N + N) and soluble reactive phosphate (SRP) were 0.03 μmol L^{-1}. DOC concentrations were measured on a Shimadzu TOC-V analyzer in high temperature catalytic oxidation mode (Wu et al., 2015). A five-point standard curve was generated using potassium hydrogen phthalate standards on a daily basis. DOC concentrations were obtained by subtracting the running blank from the average peak area of the samples (injected 3–5 times) and dividing by the slope of the standard curve. The coefficient of variation for DOC analysis based on replicate measurements was ~2%. The running blank was determined as the average of the peak area of the Milli-Q water acidified with H_3PO_4. The precision of the DOC analysis was ±0.8 μmol C L^{-1} based on DOC Consensus Reference Material (CRM) provided by D.A. Hansell from the University of Miami (https://hansell-lab.rsmas.miami.edu/consensus-reference-material/index.html). All data are reported as mean ±SD and all "differences" referred to in presentation of the results denote a statistically significant of $p < 0.05$, unless otherwise stated.

2.5. DOM Optical Measurements

Absorbance spectra for CDOM were determined using a 2310 UV-Visible spectrophotometer (Techcomp, China) equipped with a 10-cm pathlength quartz cuvette at room temperature. Absorbance scans were acquired from 240 to 800 nm with a spectral resolution of 1 nm. Milli-Q water was measured every five samples to provide a blank to correct for any baseline drift. Spectra were corrected by subtracting the absorption of Milli-Q water from the sample spectra. CDOM data are reported as Napierian absorption coefficients ($a_{CDOM}[\lambda]$) in m^{-1}, calculated as:

$$a_{\mathrm{CDOM}}(\lambda) = 2.303 \times \frac{A(\lambda)}{L}, \tag{2}$$

where $A(\lambda)$ is the absorbance (unitless) at a specified wavelength λ (nm) obtained directly from the spectrophotometer and L (m) is the cuvette pathlength (0.1 m). Absorption coefficients at 254, 325, 350, and 443 nm are reported as they have been widely reported for marine DOM samples (Iuculano et al., 2019; Nelson et al., 2010). The spectral slope over the range 275–295 nm ($S_{275-295}$) was calculated by linear regression of the natural log-transformed absorption spectra (Helms et al., 2008). Specific ultraviolet absorbance at 325 nm ($SUVA_{325}$) was calculated by dividing the decadal absorption coefficient (i.e., $A(\lambda)/L$ from Equation 2) by the DOC concentration in units of mg C L^{-1} (Hansen et al., 2016).

Fluorescence excitation-emission matrices (EEMs) were measured using a Varian Cary Eclipse spectrofluorometer according to Wang et al. (2017). Briefly, emission scans from 280 to 600 nm were recorded at 2-nm intervals with excitation wavelengths ranging from 240 to 450 nm at 5-nm intervals using a 1-cm pathlength quartz cuvette. Slit widths were 10 nm for the excitation and emission. Inner filter corrections were not applied because of the low absorbance ($A < 0.005$ at 240 nm for a 0.5-cm pathlength) for open ocean samples (Catalá et al., 2016; Yamashita et al., 2017). The EEMs were normalized and blank corrected using daily Raman spectra of freshly generated Milli-Q water; hence data are presented in Raman Units (RU) (Lawaetz & Stedmon, 2009). The coefficient of variation for the area under the water Raman peak during analyses was 1.7% ($n = 29$).

We determined two humic-like components (peak C, ex/em: 355/456 nm and peak M, ex/em: 320/400 nm) and one protein-like component (peak T, ex/em: 275/340 nm) based on contour plots, which are ubiquitous in the open ocean (Catalá et al., 2016; Coble, 1996; Jørgensen et al., 2011). The humification index (HIX) was calculated as the integrated emission spectra area at 435–480 nm divided by the sum of 300–345 nm plus 435–480 nm emission areas when excited at 254 nm (Ohno, 2002). DOC-normalized fluorescence intensity of $FDOM_H$ ($FDOM_H$*, RU m^3 g^{-1} C) was calculated by dividing the sum of peak C and peak M intensities by the DOC concentration (Hansen et al., 2016).

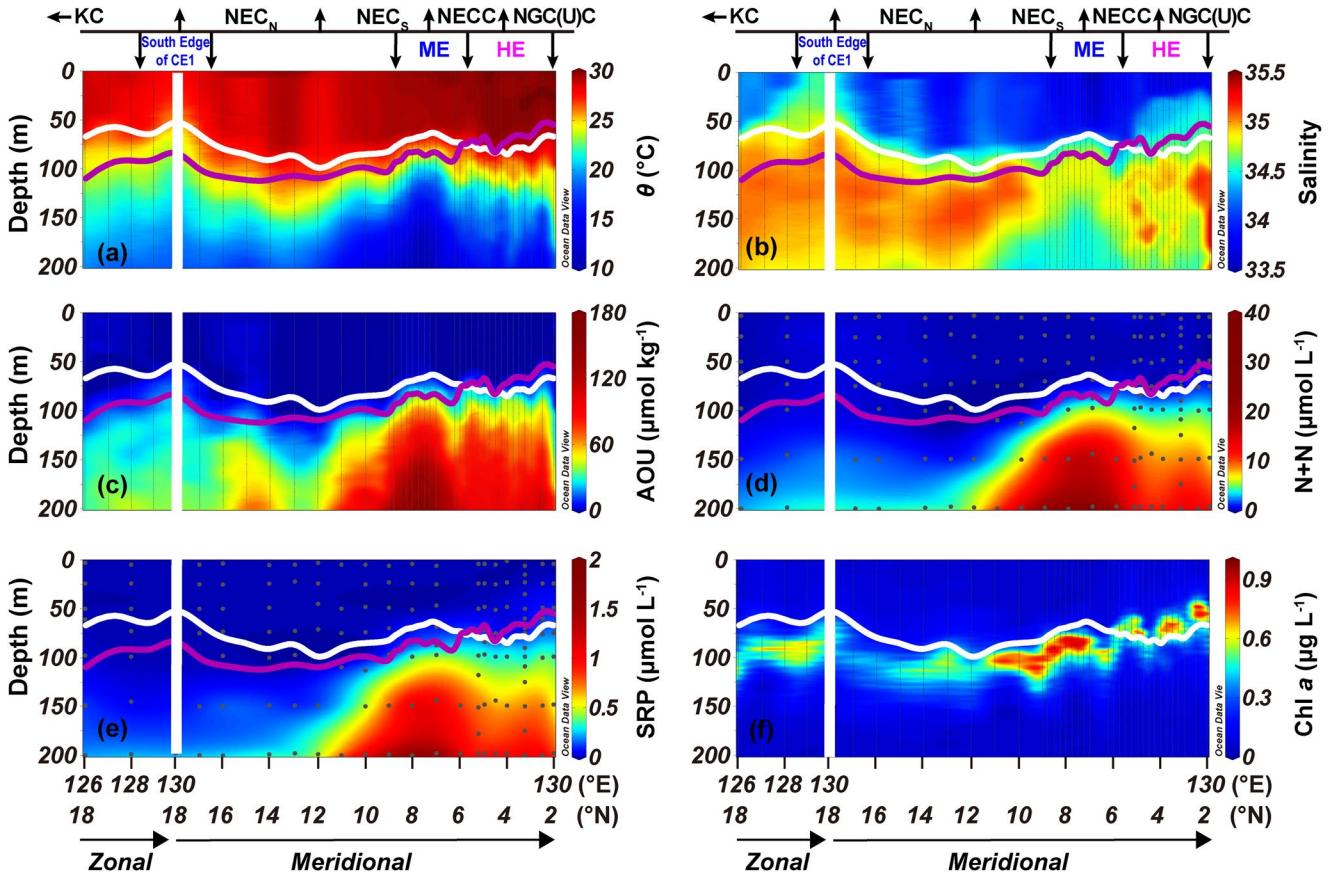

Figure 2. Sectional distributions of (a) Potential temperature (θ), (b) Salinity, (c) Apparent oxygen utilization (AOU), (d) Nitrate plus nitrite (N + N), (e) Soluble reactive phosphate (SRP) and (f) Chl *a* concentration along the zonal 18°N and meridional 130°E transects. Black dots denote the locations of biogeochemical discrete samples in subpanels (d and e). The other subpanels (a–c, f) were created using CTD sensor data (1-m interval). White and purple lines indicate the depth of the mixed layer and subsurface Chl *a* maximum (DCM) layer, respectively. Stations are divided into three currents and three eddies, and are denoted along the top. Images created using Ocean Data View (https://odv.awi.de).

3. Results

3.1. Physical, Chemical, and Biological Parameters Along the Meridional 130°E and Zonal 18°N Transects

Temperature, salinity, AOU, nutrients, and Chl *a* along the meridional 130°E and zonal 18°N transects showed a close relationship with the depth of the mixed layer (45–107 m), which was shallow in the two cold eddies (Mindanao Eddy: 67 m; south edge of CE1: 45 m), the zonal 18°N transect (59 ± 10 m), NECC (76 ± 8 m) and NGC(U)C (77 ± 9 m), and deeper in the NEC$_N$ (87 ± 14 m). The N^2 value showed decoupling within the depths of the mixed layer. A higher N^2 was found in Mindanao Eddy (0.97 min^{-2}) (*t*-test, $p < 0.05$), whereas the south edge of CE1 showed comparable N^2 values with the surrounding waters (Figure S2). N^2 was low in the zonal 18°N transect (0.56 ± 0.05 min^{-2}) and NEC$_N$ (0.63 ± 0.07 min^{-2}), but higher in the NECC (0.86 ± 0.06 min^{-2}) and NGC(U)C (0.82 ± 0.04 min^{-2}).

Potential temperature (θ) was high within the mixed layer and decreased with depth (Figure 2a). A dome-like distribution of colder θ was pronounced below the mixed layer at Mindanao Eddy and the south edge of CE1. A subsurface salinity maximum (>35) in the 90–150-m depth range was well-developed below the mixed layer, especially in NEC$_N$ and NGC(U)C (Figures 2b and S3). This layer became thinner at Mindanao Eddy due to strong upwelling of low-salinity (<34.5) North Pacific Intermediate Water. Such a dome-like, low salinity feature was absent at the south edge of CE1, whereas a higher salinity region occurred in its mixed layer (Figure 2b). The θ and salinity profiles in Halmahera Eddy were similar to the surrounding waters both within and below the mixed layer.

Dissolved oxygen was nearly saturated or slightly oversaturated in the mixed layer along both transects. Below the mixed layer, AOU generally increased with depth and ranged from 0 to 173 μmol kg^{-1} (Figure 2c). The average AOU values below the mixed layer depth for NECC (74 ± 16 μmol kg^{-1}) and NGC(U)C (67 ± 16 μmol kg^{-1}) were much higher than the NEC_N (28 ± 9 μmol kg^{-1}) and zonal 18°N transect (22 ± 3 μmol kg^{-1}) (*t*-test, $p < 0.05$). Nutrients were largely depleted in the mixed layer along both transects (<0.2 μmol N + N L^{-1} and <0.05 μmol SRP L^{-1}) (Figures 2d and 2e). Below the mixed layer, the zonal 18°N transect and NEC_N were characterized by lower nutrient concentrations (11 ± 4 μmol N + N L^{-1} and 0.8 ± 0.3 μmol SRP L^{-1}) and a deeper nutricline depth (~200 m) compared to the NECC and NGC(U)C (*t*-test, $p < 0.05$). The Mindanao Eddy, characterized by high AOU and nutrient concentrations and a dome-like nutricline, showed strong AOU and nutrient gradients at the frontal area with the NEC_S. However, there were no significant differences for AOU and nutrients among the south edge of CE1, Halmahera Eddy and the surrounding waters (*t*-test, $p > 0.05$) (Figures 2c–2e).

A subsurface Chl *a* maximum (DCM) was well developed between 47 and 113 m in the two transects, with Chl *a* concentrations ranging between 0.39 and 0.98 μg L^{-1} in this layer. The DCM was generally above the depth of the mixed layer to the south of 6°N (NGC(U)C and Halmahera Eddy) and below the mixed layer to the north (NEC and Mindanao Eddy) along the 130°E and zonal 18°N transects (Figure 2f). The DCM of NECC (0.73 ± 0.15 μg L^{-1}) and NGC(U)C (0.78 ± 0.12 mg m^{-3}) had larger Chl *a* concentrations than the NEC_N (0.53 ± 0.08 μg L^{-1}) and zonal 18°N transect (0.66 ± 0.06 μg L^{-1}) (*t*-test, $p < 0.05$). Notably, the frontal area between the NEC_S and Mindanao Eddy showed a remarkably high Chl *a* concentration (0.87 ± 0.08 μg L^{-1}) at the DCM.

3.2. DOC, CDOM, and FDOM Distributions Along the Meridional 130°E and Zonal 18°N Transects

DOC concentration varied from 50 to 81 μmol L^{-1} in the upper 200 m along the 130°E transect (Figures 3a and S4). DOC concentrations in the mixed layer were higher and varied minimally. DOC generally decreased with depth below the mixed layer, with NEC_N having a higher DOC concentration (67 ± 9 μmol L^{-1}) than NGC(U)C (58 ± 5 μmol L^{-1}) and NECC (60 ± 2 μmol L^{-1}) (*t*-test, $p < 0.05$). The $a_{CDOM}(254)$ ranged from 0.91 to 1.72 m^{-1} along both transects and displayed a subsurface maximum around the depth of the DCM (Figures 3b and S4). Within the mixed layer, the $a_{CDOM}(254)$ in NEC_N (1.13 ± 0.04 m^{-1}) was comparable to that in NECC (1.12 ± 0.05 m^{-1}), but both were slightly lower than that in the NGC(U)C (1.21 ± 0.09 m^{-1}) and zonal 18°N transect (1.20 ± 0.10 m^{-1}) (*t*-test, $p < 0.05$). Below the mixed layer, the NEC_N and zonal 18°N transect showed higher average $a_{CDOM}(254)$ (1.12 ± 0.05 m^{-1} and 1.14 ± 0.14 m^{-1}) than the NGC(U)C and NECC (1.06 ± 0.05 m^{-1}) (*t*-test, $p < 0.05$).

Strong positive correlations ($p < 0.001$, $n = 171$) were found among CDOM absorption coefficients at the three longer wavelengths ($a_{CDOM}[325]$, $a_{CDOM}[350]$, and $a_{CDOM}[443]$). Thus, for simplicity, we report only the $a_{CDOM}(325)$ results. The $a_{CDOM}(325)$ values (0.07–0.13 m^{-1}) were low in the mixed layer and generally increased with depth (Figure 3d). There was a strong vertical gradient in $a_{CDOM}(325)$ at the base of the mixed layer, which separated the water column into an upper $a_{CDOM}(325)$-depleted layer and deeper $a_{CDOM}(325)$-enriched layer (Figures 3d and S4). In the mixed layer, $a_{CDOM}(325)$ values in NGC(U)C (0.13 ± 0.01 m^{-1}) were higher than in NEC_N, NECC and zonal 18°N transect (0.09 ± 0.01–0.11 ± 0.02 m^{-1}) (*t*-test, $p < 0.05$). In contrast, $a_{CDOM}(325)$ below the mixed layer of NECC and NEC_S (0.18 ± 0.01 m^{-1}) was higher than the other currents (0.15 ± 0.02 m^{-1}–0.16 ± 0.02 m^{-1}) (*t*-test, $p < 0.05$).

The spectral slope $S_{275\text{-}295}$ (23–56 μm^{-1}) in the upper 200 m showed a contrasting vertical pattern with $a_{CDOM}(325)$, whereas $SUVA_{325}$ (0.03–0.15 m^2 g^{-1} C) and $a_{CDOM}(325)$ showed a similar pattern (Figures 3d and 3e) (Hansen et al., 2016; Helms et al., 2008). NEC_N showed the highest $S_{275\text{-}295}$ and lowest $SUVA_{325}$, both within (48 ± 4 μm^{-1} and 0.05 ± 0.01 m^2 g^{-1} C) and below (38 ± 2 μm^{-1} and 0.09 ± 0.01 m^2 g^{-1} C) the mixed layer. The lowest $S_{275\text{-}295}$ and highest $SUVA_{325}$ were found in NGC(U)C within the mixed layer (41 ± 4 μm^{-1} and 0.07 ± 0.002 m^2 g^{-1} C) and in NECC below the mixed layer (32 ± 3 μm^{-1} and 0.11 ± 0.004 m^2 g^{-1} C), respectively.

The intensity of the protein-like peak T was nearly homogeneous in the upper 200-m water column, except for a few high or extremely low values at several stations (Figure 3f). The humic-like peaks C and M

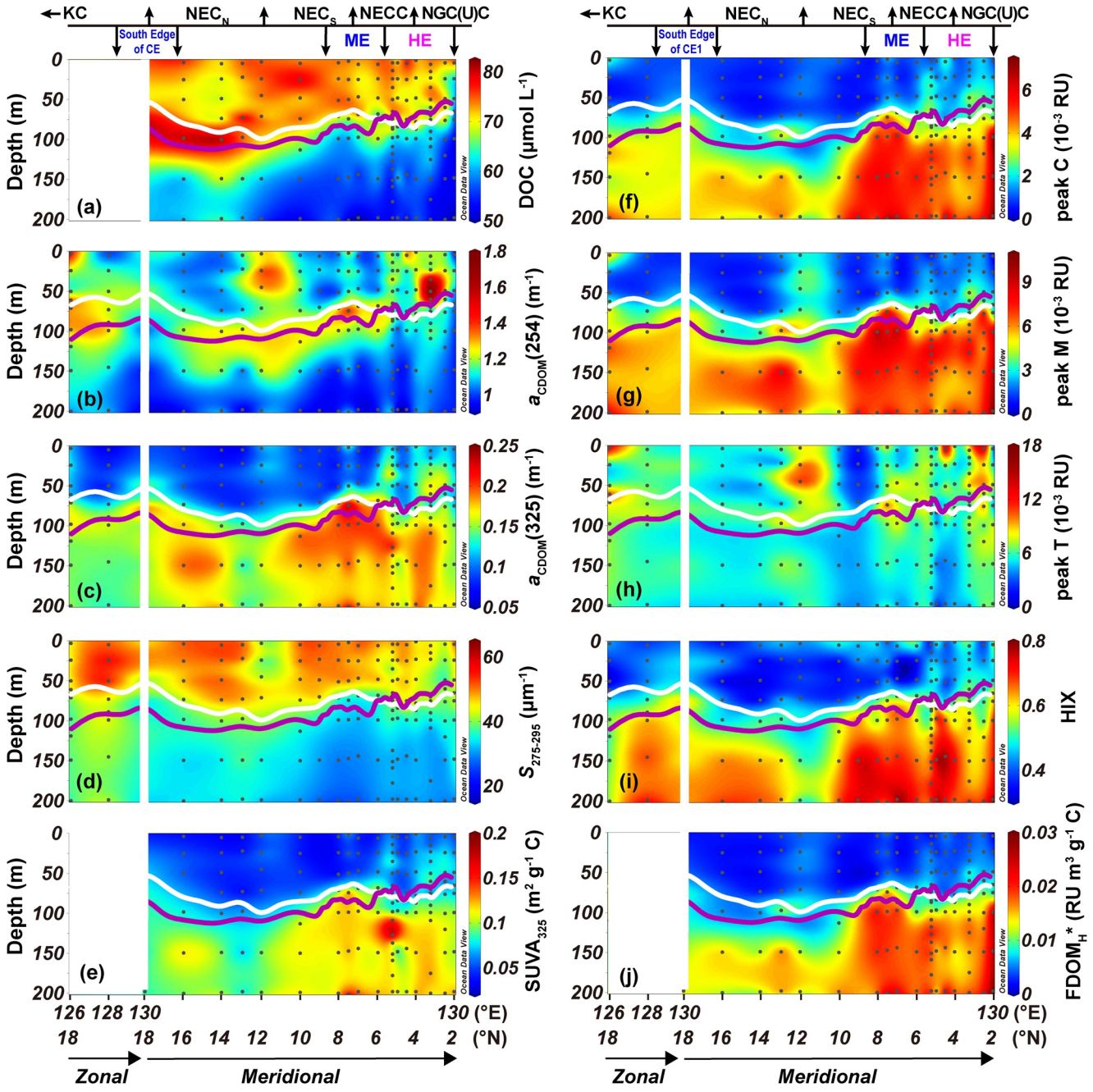

Figure 3. Sectional distributions of (a) Dissolved organic carbon (DOC), (b) $S_{275\text{-}295}$, (c) $a_{CDOM}(254)$, (d) $a_{CDOM}(325)$, (e) $SUVA_{325}$, (f) Peak T, (g) Peak C, (h) Peak M, (i) HIX and (j) Carbon-normalized humic-like FDOM ($FDOM_H$*) along the zonal 18°N and meridional 130°E transects. Black dots denote the locations of biogeochemical discrete samples. White and purple lines indicate the depth of the mixed layer and Chl *a* maximum (DCM) depth, respectively. Stations divided into three currents and three eddies as denoted along the top. Images created using Ocean Data View (https://odv.awi.de).

($FDOM_H$) were highly correlated in the upper 200 m ($r = 0.95$, $n = 174$, and $p < 0.001$). Both components had low intensities in the mixed layer and rapidly increased with depth (Figures 3g and 3h). The maximal gradient variation at the base of the mixed layer divided the water column into an upper $FDOM_H$-depleted layer and deeper $FDOM_H$-enriched layer (Figure S4). Within the mixed layer, the NEC_N and zonal 18°N transect had lower $FDOM_H$ intensity ($[2.9 \pm 1.3] \times 10^{-3}$ RU) than that in NGC(U)C ($[4.4 \pm 0.7] \times 10^{-3}$ RU) and NECC ($[3.9 \pm 1.5] \times 10^{-3}$ RU) (*t*-test, $p < 0.05$). Below the mixed layer, the NEC_N and zonal 18°N transect

had lower $FDOM_H$ intensities ([8.6 ± 2.0] × 10^{-3} RU) than NGC(U)C and NECC ([11.4 ± 1.2] × 10^{-3} RU) (*t*-test, $p < 0.05$).

HIX and DOC-normalized intensity of the humic-like peaks C and M ($FDOM_H$*) showed similar distribution patterns to $FDOM_H$ (Figures 3i and 3j). The lowest average HIX value occurred in the NEC_N and zonal 18°N transect both within (0.41 ± 0.04) and below (0.58 ± 0.07) the mixed layer. The highest average HIX value within and below the mixed layer was found in NGC(U)C (0.49 ± 0.04) and NECC (0.67 ± 0.07). NEC_N showed the lowest $FDOM_H$* both within ([3.4 ± 1.4] × 10^{-3} RU m^3 g^{-1} C) and below ([10.7 ± 2.6] × 10^{-3} RU m^3 g^{-1} C) the mixed layer, whereas NGC(U)C had its highest $FDOM_H$* within ([5.2 ± 0.6] × 10^{-3} RU m^3 g^{-1} C) and below ([16.7 ± 3.4] × 10^{-3} RU m^3 g^{-1} C) the mixed layer.

Dome-like isolines for DOC, CDOM, and FDOM were pronounced in Mindanao Eddy and the south edge of CE1 compared to the surrounding waters (Figure 3). As a result, DOC, CDOM, and FDOM showed large vertical gradients in the frontal area at NEC_S (Figure 3). Levels of DOC, $a_{CDOM}(254)$, $a_{CDOM}(325)$, and peaks T, C and M in the Mindanao Eddy were significantly higher than in the surrounding waters below the mixed layer (*t*-test, $p < 0.05$). Consistently lower $S_{275\text{-}295}$ and higher $SUVA_{325}$, HIX and $FDOM_H$* were also observed in the Mindanao Eddy below the mixed layer (*t*-test, $p < 0.05$). However, these parameters were comparable to the surrounding waters in the mixed layer (*t*-test, $p > 0.05$). At the south edge of the CE1 mixed layer, there were no statistic differences for DOC, $a_{CDOM}(254)$, $a_{CDOM}(325)$, and peak C and M levels compared to those in the surrounding waters (*t*-test, $p > 0.05$). Below the mixed layer, only lower $a_{CDOM}(254)$ was found in the south edge of CE1 versus the surrounding waters (*t*-test, $p < 0.05$). There were no significant differences between DOC, CDOM, and FDOM parameters between the core and edge areas of Halmahera Eddy, either within or below the mixed layer (*t*-test, $p > 0.05$) (Figure 3).

4. Discussion

4.1. Factors Shaping the Epipelagic Profiles of DOC and DOM Optical Properties

Four distinct vertical patterns were observed for bulk DOC and optical properties of DOM in the tropical Northwest Pacific (Figure 3), inferring that their distributions in the epipelagic ocean are subject to multiple biogeochemical processes once produced by photosynthesis (Carlson & Hansell, 2015). The DOC profile monotonously decreased with depth and was unique from all other CDOM and FDOM parameters (Figure 3). The station-averaged DOC concentration was negatively correlated with the squared Brunt-Väisälä frequency (N^2, $r = -0.68$, and $p = 0.003$, Figure 4a), but not correlated with Chl *a* ($p > 0.05$), suggesting that the water column stability has a strong influence on DOC distribution of the upper ocean. The $a_{CDOM}(254)$ profile displayed a subsurface maximum coincident with the DCM layer as corroborated by the positive relationship between station-averaged $a_{CDOM}(254)$ and Chl *a* in the subsurface maximum zone (50–150 m) ($r = 0.67$, $p = 0.002$, Figure 4b). Since $a_{CDOM}(254)$ is purported to correspond to absorbance by relatively small, simple compounds (conjugated carbon double bonds) (Lakowicz, 2006; Lønborg et al., 2015), the positive relationship between $a_{CDOM}(254)$ and Chl *a* infers that $a_{CDOM}(254)$ could be used as an indicator for the relatively bio-labile pool of DOM (Guallar & Flos, 2019; Lønborg et al., 2015). Recent studies in the Northeast Atlantic Ocean and Mediterranean Sea indicated that $a_{CDOM}(254)$ was an effective proxy for DOC concentrations in the open ocean (Catalá et al., 2018; Galletti et al., 2019). However, $a_{CDOM}(254)$ in this study explained only 36% of the variance in DOC concentrations in the upper 200-m water column. These results indicate that $a_{CDOM}(254)$ was not a good proxy for DOC in the tropical epipelagic Northwest Pacific, which may result from the DOC in the upper ocean containing a large proportion of non-chromophoric compounds (e.g., carbohydrates, amino acids) (Kaiser & Benner, 2009) whose behaviors are primarily regulated by physical processes. The inventory of peak T in the upper 200-m water column showed a weak positive correlation with Chl *a* inventory ($r = 0.54$, $p = 0.02$, Figure 4c). This result is consistent with a previous culture experiment that demonstrated primary production contributed to peak T fluorescence (Nieto-Cid et al., 2006).

The $a_{CDOM}(325)$ and $FDOM_H$ showed similar vertical distributions and strong correlations ($r > 0.80$, $p < 0.001$). The most prominent features for these parameters were sharp vertical gradients near the base of the mixed layer. Above the mixed layer, $a_{CDOM}(325)$ and $FDOM_H$ were highly depleted and homogeneous due to strong photobleaching (Helms et al., 2013), which was also consistent with the high $S_{275\text{-}295}$

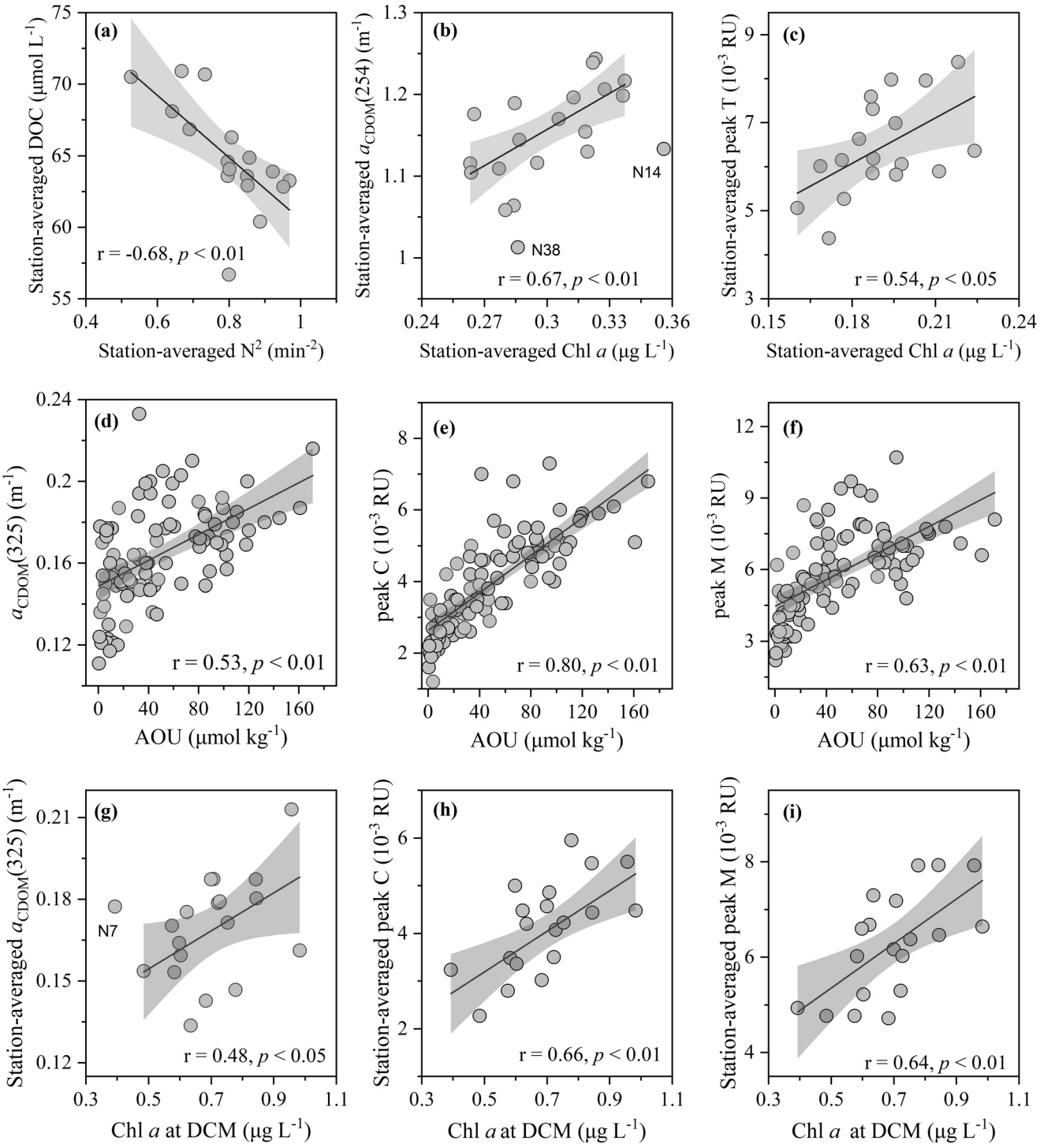

Figure 4. Relationships between dissolved organic matter (DOM) properties and water quality/hydrodynamic parameters. (a) Station-averaged dissolved organic carbon concentration in the upper 200 m versus the squared Brunt-Väisälä frequency (N^2) in the upper 200 m; (b) Station-averaged $a_{CDOM}(254)$ in the depth range of 50–150 m versus Chl *a* in the subsurface maximum layer (50–150 m); (c) Station-averaged intensity of peak T in the upper 200 m versus station-averaged Chl *a* in the upper 200 m; (d)–(f) The field-measured $a_{CDOM}(325)$, peak C and peak M versus apparent oxygen utilization below the mixed layer; (g)–(i) Station-averaged $a_{CDOM}(325)$, peak C and peak M below the mixed layer versus Chl *a* concentration at Chl *a* maximum layer. Black lines and gray shadows represent the linear fit lines and 95% confidence bands. Three outlier points are labeled and were excluded from the analysis.

(Figures 3d, 3e and 3j). These components accumulate below the mixed layer resulting in a simultaneous increase of HIX and $SUVA_{325}$ (Figure 3e). Their values showed positive relationships with Chl *a* concentration at the DCM and with AOU below the mixed layer (Figures 4d–4i). This evidence indicates that these components are associated with microbial metabolism of sinking biogenic materials in the nutrient-depleted, lower euphotic layer, thereby representing relatively bio-refractory DOM fractions (Guallar & Flos, 2019; Iuculano et al., 2019; Jørgensen et al., 2014; Romera-Castillo et al., 2010). This interpretation is consistent with results from a global-scale, generalized additive model that determined AOU and Chl *a* to have the largest effects on the distribution of humic-like fluorescence in the epipelagic ocean (Catalá et al., 2016). Thus, vertical DOM profiles represent interactive responses to production and degradation (photochemical and biological) processes in the epipelagic tropical Northwest Pacific.

4.2. Vertical Transport of DOC, CDOM, and FDOM by Mesoscale Eddies

Two quasi-permanent mesoscale eddies (cold Mindanao and warm Halmahera) and one transient cold eddy (CE1) showed contrasting vertical distributions of DOM parameters (Figure 3). The lower sea surface height at the core of the Mindanao Eddy and south edge of CE1 suggests a strong upwelling (eddy pumping) in the eddy interior (Figure 1a). For Mindanao Eddy, significantly higher $a_{CDOM}(325)$, CDOM, and $FDOM_H$ values were found below the mixed layer compared to the surrounding waters. These elevated values were not apparent within the mixed layer suggesting that the upward transport of photo-sensitive DOM compounds from the deeper ocean was restricted to below the mixed layer as a result of stable stratification conditions within the cold eddy area (Figure S2). However, mesoscale eddy processes along the edges of the convergence frontal area between Mindanao Eddy and NEC_S may contribute to the asymmetrically higher DCM Chl *a* concentrations, and therefore to the addition of phytoplankton-derived DOM materials (Figures 2c, 3b and 3f). These processes mix the phytoplankton through near-surface eddy advection, mostly along the eddy periphery (Chelton et al., 2011; Gaube et al., 2014; He et al., 2016). Unlike the Mindanao Eddy, the south edge of CE1 showed elevated $a_{CDOM}(325)$ and FDOM in the mixed layer. This suggests enhanced diapycnal mixing along the south edge of CE1 that entered the pycnocline creating the surface salinity maximum and concurrent alterations to DOM patterns in the mixed layer. Similar patterns were previously documented for cold eddies in the South China Sea (Wang et al., 2017).

The warm Halmahera Eddy showed a comparable sea surface height to its surrounding waters, thereby suggesting a weak downwelling system inside the eddy (Figure 1a). As a result, inventories of Chl *a* and nutrients, as well as DOC, CDOM, and FDOM, in the upper 200 m of the Halmahera Eddy region were similar to those in the surrounding waters (Figures 2 and 3). Hence, the warm Halmahera Eddy showed minimal effects on the downward transport of DOM, although it was active during the cruise period (Figure 1a). These findings are in sharp contrast to warm eddies in the marginal South China Sea where DOC enrichment and $FDOM_H$ deficits occur inside the eddy core area, with associated enhancement of export productivity at the eddy edge (Wang et al., 2017; Zhou et al., 2013).

4.3. Lateral Variation of DOM Pools in the Three Currents Along the 130°E Transect

The northern NEC_N and NGC(U)C input currents along the 130°E transect contained two-separate layers with respect to nutrients, $a_{CDOM}(325)$ and $FDOM_H$ (Figures 2e, 2f and 3). In the mixed layer, the NEC_N showed comparable levels of DOC and peak T, lower $a_{CDOM}(254)$, $a_{CDOM}(325)$ and $FDOM_H$ levels compared to the NGC(U)C (Figure 5). The higher $S_{275\text{-}295}$ and lower HIX, $SUVA_{325}$ and $FDOM_H$* values observed in NEC_N versus NGC(U)C demonstrate that the DOM in the NEC source area was highly photodegraded with a lower average molecular weight, humification degree, and aromaticity. The NEC_N in this study showed similar DOC-rich, $a_{CDOM}(325)$-depleted, and $FDOM_H$-depleted features to the Kuroshio Current to the east of the Luzon Strait (Wang et al., 2017; Wu et al., 2015). As the N-rich DOM in the Kuroshio Current is readily consumed by bacteria when entering the nutrient-rich South China Sea (Xu et al., 2018), we posit that DOM in the mixed layer of the NEC may have similarly high microbial utilization potential.

The NGC(U)C represents the features of water masses from the South Pacific and flows close to the land (Figure 1a). Thus, it has a greater opportunity to receive humic materials from the land and shelf area. These humic materials may be responsible for the higher $a_{CDOM}(325)$ and $FDOM_H$ in the mixed layer of

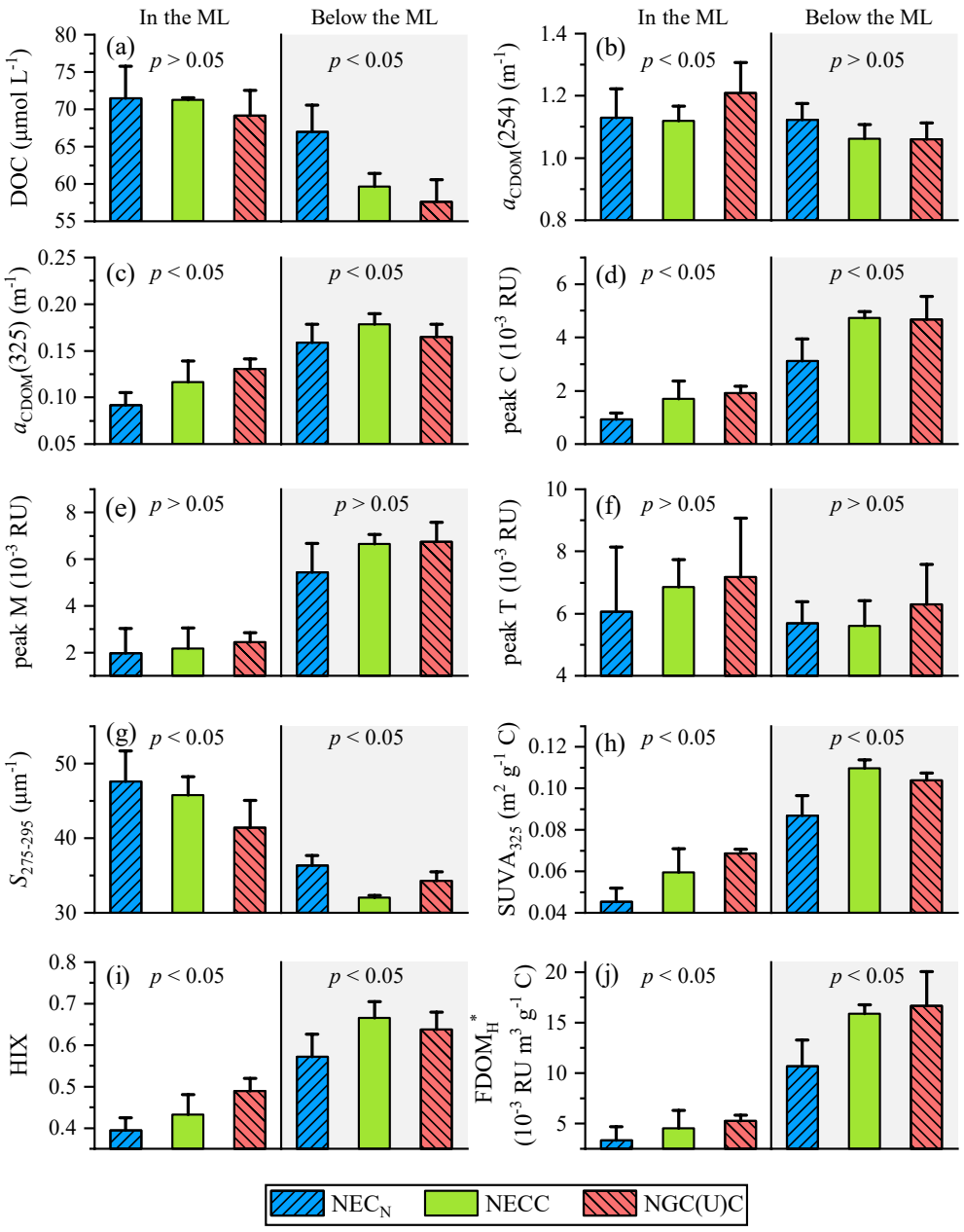

Figure 5. Comparison of dissolved organic carbon (DOC), chromophoric dissolved organic matter (CDOM), and fluorescent dissolved organic matter (FDOM) parameters among three currents (North Equatorial Current$_N$, North Equatorial Countercurrent, and New Guinea Coastal Current and Undercurrent) in and below the mixed layer (ML). Columns and error bars represent the averages and standard deviations of DOC, CDOM, and FDOM for all stations within a given current system. The significance levels for difference of averages among three currents are labeled at the top of columns.

NGC(U)C. The higher levels of $a_{CDOM}(254)$ in the mixed layer of NGC(U)C were more likely sourced from enhanced primary production (Huang et al., 2019). Although the mixed layer of NGC(U)C was characterized as nutrient-depleted like the NEC$_N$ (Figures 2e and 2f), its slower water mixing due to lower wind shear could lead to a greater Chl *a* inventory in the DCM layer located above the base of the mixed layer (Figure 2c), thus contributing to an increase of phytoplankton-sourced components (Figures 4b and 4c).

Below the mixed layer, the NEC$_N$ consisting of North Pacific Tropical Water showed lower AOU and nutrient concentrations than the NGC(U)C dominated by South Pacific Tropical Water (Figures 2d–2f) (Qu

et al., 1999; Zhou et al., 2010). This suggests that DOM below the mixed layer of the NEC_N experiences less microbial reprocessing (Huang et al., 2019). The lower microbial processing concept is fully consistent with the higher DOC, $a_{CDOM}(254)$ and $S_{275\text{-}295}$ values, but lower $a_{CDOM}(325)$, $FDOM_H$, HIX and $FDOM_H$* levels in the NEC_N compared to the NGC(U)C (Figure 5). The higher community respiration and bacterial production below the mixed layer of the NGC(U)C (Huang et al., 2019) result in higher AOU and nutrient concentrations (Figures 2d–2f). This further contributes to more highly microbially processed DOM compounds having a lower carbon content and higher average molecular weight and humification degree (Figure 5).

The NECC is the largest export pathway in the tropical Northwest Pacific (Qiu & Lukas, 1996; Qu et al., 1998). In the mixed layer, the moderate levels of DOC, CDOM, and FDOM in the NECC compared to the NEC and NGC(U)C currents suggest that its DOM pool is affected by appreciable lateral water mass mixing. Alternatively, loss of DOM to biological degradation is deemed minimal due to the low nutrient levels that limit microbial activity (Figures 2c–2f). Below the mixed layer, the NECC showed higher $a_{CDOM}(325)$, $FDOM_H$, HIX and $SUVA_{325}$ levels, and lower $S_{275\text{-}295}$ values compared to the NEC and NGC(U)C waters (Figure 5). This infers that processes other than direct lateral mixing of NEC and NGC(U)C waters regulate the DOM quality and quantity of the NECC. As the NECC is found at the frontal area between the Mindanao and Halmahera eddy pair, the upwelling driven by this strong cold eddy injects considerable nutrients that in turn enhance microbial activities and corresponding alterations to DOM pools below the mixed layer of the NECC (Figure 3) (Huang et al., 2019). These factors contributed to the NECC having the highest aromatic degree for DOM accumulated below the mixed layer among the three investigated currents.

4.4. Estimates of Lateral DOC Transport Flux in the Upper 200 m: Significance of Eddy Processes

4.4.1. Lateral DOC Flux Estimated by Mass Balance Model

The main currents of the tropical Northwest Pacific fall within an area bounded by the zonal 18°N and meridional 130°E transects, the Philippine Islands to the west and Indonesia to the south (Figure 1a). Given that vertical velocities are at least an order-of-magnitude lower than lateral velocities in this system (Figure S5) and there are no large river inputs to this system (Raymond & Spencer, 2015), a constrained mass balance for lateral water (volume) transport is expected. We also assume that DOC diffusion fluxes are negligible compared to the much larger lateral DOC transport processes (Hansell et al., 2009). Thus, a simplified mass balance model was developed to estimate the DOC budget for the study area:

$$\sum_{i=1}^{n} Q_i \times \mathrm{DOC}_i = 0, \tag{3}$$

where Q_i represents the volume transport for inputs (+, northern NEC [12°N–17°N], southern NEC [7.5°N–12°N], and NGC(U)C) and outflows (−, NECC, Kuroshio Current, and Indonesian Throughflow) over the upper 200 m of the tropical Northwest Pacific. HYCOM-simulated average velocity data were available for the entire cruise period (October 25–November 12, 2017). The HYCOM-velocity data were comparable to field-observed velocity data acquired by the shipboard Acoustic Doppler Current Profile (SADCP) between 50 and 200 m (Figure 6). Thus, we used the HYCOM-velocity data for the calculation of lateral volume transport (Q_i). Except for unknown data from the Indonesian Throughflow, DOC concentrations for the end-members (NEC, NECC, and NGC(U)C) and the Kuroshio Current were available from this study and previously published results (Wu et al., 2015).

Model results indicated that DOC transport fluxes from the central Pacific into the tropical Northwest Pacific by the NEC_S (1.9 ± 0.9 Tg C d^{-1}), the frontal area associated with the Mindanao Eddy, was six times higher than the NEC_N (0.3 ± 0.2 Tg C d^{-1}) (Figure 7). This demonstrates that eddy processes can greatly enhance lateral DOC transport in the western boundary current system. The DOC inputs from the NEC_N were subsequently exported by the Kuroshio Current, influencing the carbon biogeochemistry in marginal seas (e.g., South China Sea, East China Sea) and the subtropical and subpolar Pacific (Ding et al., 2019; Xu et al., 2018; Yamashita et al., 2017).

The westward-flowing Indonesian Throughflow is the only low-latitude inter-ocean current, flowing from the Equatorial Pacific Ocean into the southeastern Indian Ocean. Our model estimated a DOC transport

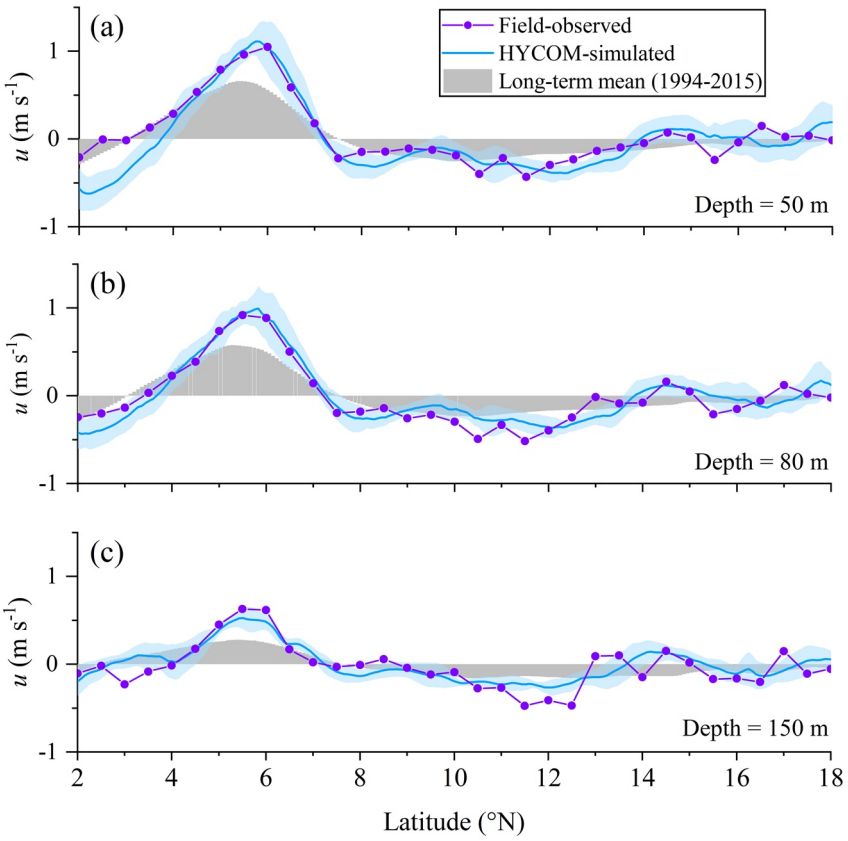

Figure 6. Comparison of field-observed, simulated, and long-term average zonal velocity (u) at depths of 50, 80, and 150 m along the 130°E transect. Field-observed velocity (purple dots) was measured using a shipboard Acoustic Doppler Current Profiler at a frequency of 38 kHz. Hybrid Coordinate Ocean Model (HYCOM)-simulated velocity (blue line) represents the average value during the cruise period (October 25 to November 12, 2017). The long-term average velocity (gray shadow) was the average value from 1994 to 2015 for the same season (October to November) as simulated by HYCOM.

flux and average DOC concentration for the Indonesian Throughflow of 0.8 ± 1.0 Tg C d^{-1} and ~64 μmol L^{-1}, respectively (Figure 7). This flux could increase when river inputs from Indonesian Islands converge along its pathway. Although this estimate may have some uncertainties from disregarding the vertical transport and diffusive terms, such a flux estimate is deemed reasonable as no large fluvial DOM discharge exists (e.g., from west Australia) in the southeastern Indian Ocean (Raymond & Spencer, 2015). Lack of strong terrestrial contributions make this "source" flux of great importance to the biogeochemistry of the receiving Indian Ocean.

4.4.2. Comparison of the 2017 Lateral DOC Budget to the Long-Term (1994–2015) Average

Past hydrological observations demonstrated that the quasi-permanent Mindanao and Halmahera eddy pair and associated instabilities exert considerable impacts on lateral material transport in the study area (Kashino et al., 2013; Liu et al., 2021). To quantify the contributions of Mindanao and Halmahera eddy transport on lateral DOC fluxes across the 130°E transect specifically relevant to the eddy pair, we compared 2017 current velocities with the long-term (1994–2015) climatological average velocities during the cruise period (October–November) based on the 22-years data-assimilative HYCOM NCODA product. This product effectively assimilates satellite altimetry and other miscellaneous observations to create a long record of ocean circulation fields (Chassignet et al., 2007). The long-term average circulation field eliminates high-frequency fluctuations of latitudinal displacements for the Mindanao and Halmahera eddy pair, as well as the effects from transient eddies. Hence, the NEC_N, NECC, and NGC(U)C may be viewed as static current systems (Liu et al., 2021). In a sense, the current anomalies, obtained by subtracting the long-term average from the 2017 currents, represent the eddy transport anomalies associated with eddy activities and upstream

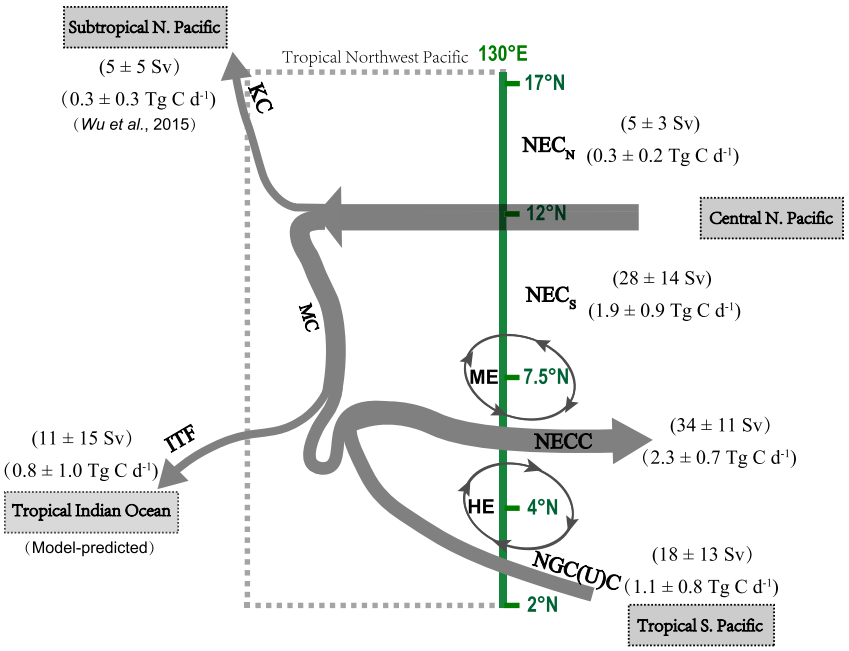

Figure 7. Estimates of lateral dissolved organic carbon transport flux in the epipelagic tropical Northwest Pacific. Note: 1 Sv = 10^6 m^3 s^{-1}.

processes. For example, some anomalies may be closely associated with modes of the 2017 La Niña event. Thus, DOC transport anomalies can be estimated by assuming that the 2017 DOC concentrations from the study area were not different from the long-term average.

The average zonal velocity (-0.02 ± 0.15 m^{-1}) and therefore volume transport flux by the NEC_N over the cruise period showed a comparable magnitude to the climatology-based velocity (-0.09 ± 0.03 m^{-1}). This infers that transient eddies have a limited effect on lateral DOM transport along the northern edge of the 130°E transect. The contributions of eddy and upstream processes to lateral DOC transport fluxes of the NEC_S, NECC, and NGC(U)C currents accounted for 38%, 40% and 46% of the total flux during the cruise period, respectively. This implies that eddy activities associated with the instability of the Mindanao and Halmahera eddy pair played an important role in lateral DOM transport dynamics of the tropical Northwest Pacific. In particular, current anomalies accelerated the transport of DOC sourced from the South Pacific into the eastward-flowing NECC (2.3 ± 0.7 Tg C d^{-1}) by the narrow northwestward-flowing NGC(U)C (1.1 ± 0.8 Tg C d^{-1}). As a result, the NECC is enriched in aromatic carbon (higher absorbance and $FDOM_H$) compared to the westward-flowing NEC, which may affect the underwater light field and related ecological processes in the central equatorial Pacific. Further study is required to quantify the high-resolution variability of the Mindanao and Halmahera eddy pair on lateral DOM transport at seasonal, interannual and longer time scales (e.g., El Niño and La Niña events). Further, we assumed that the background DOC concentrations in 2017 were similar to the long-term average. There also may be discrepancies in our calculations associated with regime shifts in the DOM, which may account for eddy transport of DOM as well. Thus, future research can constrain several of our model assumptions and provide critical data to assess the consequences of hydrodynamic and biogeochemical variability (spatial and temporal) on modeled fluxes.

5. Conclusions

This study demonstrated large vertical and horizontal DOM variations in the surface layer (<200 m) of the western boundary current system of the tropical Northwest Pacific. High spatial-resolution observations revealed four distinct vertical patterns for DOC, CDOM, and FDOM parameters, which were jointly regulated by physical processes, phytoplankton production, photochemical reactions and microbial processes. DOC-enriched and $FDOM_H$-depleted NEC waters from the central Pacific and DOC-depleted

and $FDOM_H$-enriched NGC(U)C waters from the South Pacific converged to supply DOM to the tropical Northwest Pacific. These water inputs dominate the overall quantity and quality of DOM in the NECC flowing back to the central Pacific. A mass balance model using HYCOM-simulated velocity data during the cruise period revealed that the western boundary current system had large DOM exchange fluxes with altered DOM properties to the open North Pacific and Indian Ocean, thereby emphasizing the importance of lateral DOM alteration and transport in the regional oceanic carbon cycle. The quasi-permanent Mindanao and Halmahera eddy pair had different regulating effects on DOM profiles, but both enhanced lateral DOM transport fluxes carried by the NEC, NECC, and NGC(U)C. Because of the dynamic nature in water exchange predicted for the tropical Northwest Pacific under various climate change scenarios (Feng et al., 2017), further studies are needed to elucidate such climate-driven influences/feedbacks on the marine carbon cycle.

Conflict of Interest

The authors declare no conflicts of interest relevant to this study.

Data Availability Statement

The data and samples were collected by R/V *KEXUE*. All data associated with this work will be available in the Mendeley Data Repository (http://dx.doi.org/10.17632/g9m2gphz33.3#file-ed97758b-e164-4811-8816-49a52f70e3da).

Acknowledgments
This work was jointly supported by National Natural Science Foundation of China (41876083, U1805241), Senior User Project of R/V *KEXUE* (KEXUE2017G11, KEXUE2018G03), and Fundamental Research Funds for the Universities of China (20720190105). The authors are grateful to the captain, crew, technicians, and scientists for their assistance during the cruise. The author especially thank the chief scientist D. Yuan for cruise organization, Y. Sun for nutrient measurements, and L. Chen, W. Yang, and J. Xu for technical support. The authors would like to thank Prof. Shu-ji Kao, Dr. R. Cai, and X. Liu for their valuable suggestions. The authors thank Dr. P. Kowalczuk and an anonymous reviewer for their insightful comments.

References

Arruda, W. Z., & Nof, D. (2003). The Mindanao and Halmahera eddies—Twin eddies induced by nonlinearities. *Journal of Physical Oceanography*, *33*(12), 2815–2830. https://doi.org/10.1175/1520-0485(2003)033<2815:tmahee>2.0.co;2

Benson, B. B., & Krause, D. (1984). The concentration and isotopic fractionation of oxygen dissolved in fresh-water and seawater in equilibrium with the atmosphere. *Limnology & Oceanography*, *29*(3), 620–632. https://doi.org/10.4319/lo.1984.29.3.0620

Cai, R. H., Zhou, W., He, C., Tang, K., Guo, W., Shi, Q., et al. (2019). Microbial processing of sediment-derived dissolved organic matter: Implications for its subsequent biogeochemical cycling in overlying seawater. *Journal of Geophysical Research: Biogeosciences*, *124*, 3479–3490. https://doi.org/10.1029/2019JG005212

Carlson, C. A., & Hansell, D. A. (2015). Chapter 3—DOM sources, sinks, reactivity, and budgets. In D. A. Hansell, & C. A. Carlson (Eds.), *Biogeochemistry of marine dissolved organic matter* (2nd ed., pp. 65–126). Academic Press. https://doi.org/10.1016/B978-0-12-405940-5.00003-0

Carpenter, J. H. (1965). The Chesapeake Bay Institute technique for the Winkler dissolved oxygen method. *Limnology & Oceanography*, *10*(1), 141–143. https://doi.org/10.4319/lo.1965.10.1.0141

Catalá, T. S., Álvarez-Salgado, X. A., Otero, J., Iuculano, F., Companys, B., Horstkotte, B., et al. (2016). Drivers of fluorescent dissolved organic matter in the global epipelagic ocean. *Limnology & Oceanography*, *61*(3), 1101–1119. https://doi.org/10.1002/lno.10281

Catalá, T. S., Martínez-Pérez, A. M., Nieto-Cid, M., Alvarez, M., Otero, J., Emelianov, M., et al. (2018). Dissolved organic matter (DOM) in the open Mediterranean Sea I: Basin-wide distribution and drivers of chromophoric DOM. *Progress in Oceanography*, *165*, 35–51. https://doi.org/10.1016/j.pocean.2018.05.002

Chassignet, E. P., Hurlburt, H. E., Smedstad, O. M., Halliwell, G. R., Hogan, P. J., Wallcraft, A. J., et al. (2007). The HYCOM (hybrid coordinate ocean model) data assimilative system. *Journal of Marine Systems*, *65*(1–4), 60–83. https://doi.org/10.1016/j.jmarsys.2005.09.016

Chelton, D. B., Gaube, P., Schlax, M. G., Early, J. J., & Samelson, R. M. (2011). The influence of nonlinear mesoscale eddies on near-surface oceanic chlorophyll. *Science*, *334*(6054), 328–332. https://doi.org/10.1126/science.1208897

Coble, P. G. (1996). Characterization of marine and terrestrial DOM in seawater using excitation emission matrix spectroscopy. *Marine Chemistry*, *51*(4), 325–346. https://doi.org/10.1016/0304-4203(95)00062-3

Ding, L., Ge, T. T., & Wang, X. C. (2019). Dissolved organic carbon dynamics in the East China Sea and the northwest Pacific Ocean. *Ocean Science*, *15*, 1177–1190. https://doi.org/10.5194/os-15-1177-2019

Donguy, J. R., & Meyers, G. (1996). Mean annual variation of transport of major currents in the tropical Pacific Ocean. *Deep Sea Research Part I: Oceanographic Research Papers*, *43*(7), 1105–1122. https://doi.org/10.1016/0967-0637(96)00047-7

Feng, M., Zhang, X. B., Sloyan, B., & Chamberlain, M. (2017). Contribution of the deep ocean to the centennial changes of the Indonesian Throughflow. *Geophysical Research Letters*, *44*(6), 2859–2867. https://doi.org/10.1002/2017gl072577

Galletti, Y., Gonnelli, M., Retelletti Brogi, S., Vestri, S., & Santinelli, C. (2019). DOM dynamics in open waters of the Mediterranean Sea: New insights from optical properties. *Deep Sea Research Part I: Oceanographic Research Papers*, *144*, 95–114. https://doi.org/10.1016/j.dsr.2019.01.007

Gaube, P., McGillicuddy, D. J., Jr., Chelton, D. B., Behrenfeld, M. J., & Strutton, P. G. (2014). Regional variations in the influence of mesoscale eddies on near-surface chlorophyll. *Journal of Geophysical Research: Oceans*, *119*(12), 8195–8220. https://doi.org/10.1002/2014jc010111

Gordon, A. L., & Fine, R. A. (1996). Pathways of water between the Pacific and Indian oceans in the Indonesian seas. *Nature*, *379*(6561), 146–149. https://doi.org/10.1038/379146a0

Guallar, C., & Flos, J. (2019). Linking phytoplankton primary production and chromophoric dissolved organic matter in the sea. *Progress in Oceanography*, *176*, 102116. https://doi.org/10.1016/j.pocean.2019.05.008

Guo, W., Stedmon, C. A., Han, Y., Wu, F., Yu, X., & Hu, M. (2007). The conservative and non-conservative behavior of chromophoric dissolved organic matter in Chinese estuarine waters. *Marine Chemistry*, *107*(3), 357–366. https://doi.org/10.1016/j.marchem.2007.03.006

Hansell, D. A., Carlson, C. A., Repeta, D. J., & Schlitzer, R. (2009). Dissolved organic matter in the ocean: A controversy stimulates new insights. *Oceanography*, *22*(4), 202–211. https://doi.org/10.5670/oceanog.2009.109

Hansen, A. M., Kraus, T. E. C., Pellerin, B. A., Fleck, J. A., Downing, B. D., & Bergamaschi, B. A. (2016). Optical properties of dissolved organic matter (DOM): Effects of biological and photolytic degradation. *Limnology & Oceanography*, *61*(3), 1015–1032. https://doi.org/10.1002/lno.10270

He, Q., Zhang, H., Cai, S., & Zha, G. (2016). On the asymmetry of eddy-induced surface chlorophyll anomalies in the southeastern Pacific: The role of eddy-Ekman pumping. *Progress in Oceanography*, *141*, 202–211. https://doi.org/10.1016/j.pocean.2015.12.012

Helms, J. R., Stubbins, A., Perdue, E. M., Green, N. W., Chen, H., & Mopper, K. (2013). Photochemical bleaching of oceanic dissolved organic matter and its effect on absorption spectral slope and fluorescence. *Marine Chemistry*, *155*, 81–91. https://doi.org/10.1016/j.marchem.2013.05.015

Helms, J. R., Stubbins, A., Ritchie, J. D., Minor, E. C., Kieber, D. J., & Mopper, K. (2008). Absorption spectral slopes and slope ratios as indicators of molecular weight, source, and photobleaching of chromophoric dissolved organic matter. *Limnology & Oceanography*, *53*(3), 955–969. https://doi.org/10.4319/lo.2008.53.3.0955

Hu, D. X., Wu, L., Cai, W., Gupta, A. S., Ganachaud, A., Qiu, B., et al. (2015). Pacific western boundary currents and their roles in climate. *Nature*, *522*(7556), 299–308. https://doi.org/10.1038/nature14504

Huang, Y., Chen, B., Huang, B., Zhou, H., & Yuan, Y. (2019). Potential overestimation of community respiration in the western Pacific boundary ocean: What causes the putative net heterotrophy in oligotrophic systems? *Limnology & Oceanography*, *64*(5), 2202–2219. https://doi.org/10.1002/lno.11179

Iuculano, F., Álverez-Salgado, X. A., Otero, J., Catalá, T. S., Sobrino, C., Duarte, C. M., & Agustí, S. (2019). Patterns and drivers of UV absorbing chromophoric dissolved organic matter in the euphotic layer of the open ocean. *Frontiers in Marine Science*, *6*, 320. https://doi.org/10.3389/fmars.2019.00320

Jiao, N., Zhang, Y., Zhou, K., Li, Q., Dai, M., Liu, J., et al. (2014). Revisiting the CO_2 "source" problem in upwelling areas—A comparative study on eddy upwellings in the South China Sea. *Biogeosciences*, *11*(9), 2465–2475. https://doi.org/10.5194/bg-11-2465-2014

Jørgensen, L., Stedmon, C. A., Granskog, M. A., & Middelboe, M. (2014). Tracing the long-term microbial production of recalcitrant fluorescent dissolved organic matter in seawater. *Geophysical Research Letters*, *41*(7), 2481–2488. https://doi.org/10.1002/2014gl059428

Jørgensen, L., Stedmon, C. A., Kragh, T., Markager, S., Middelboe, M., & Sondergaard, M. (2011). Global trends in the fluorescence characteristics and distribution of marine dissolved organic matter. *Marine Chemistry*, *126*(1–4), 139–148. https://doi.org/10.1016/j.marchem.2011.05.002

Kaiser, K., & Benner, R. (2009). Biochemical composition and size distribution of organic matter at the Pacific and Atlantic time-series stations. *Marine Chemistry*, *113*(1–2), 63–77. https://doi.org/10.1016/j.marchem.2008.12.004

Kashino, Y., Atmadipoera, A., Kuroda, Y., & Lukijanto (2013). Observed features of the Halmahera and Mindanao Eddies. *Journal of Geophysical Research: Oceans*, *118*(12), 6543–6560. https://doi.org/10.1002/2013jc009207

Kowalczuk, P., Tilstone, G. H., Zabłocka, M., Röttgers, R., & Thomas, R. (2013). Composition of dissolved organic matter along an Atlantic meridional transect from fluorescence spectroscopy and parallel factor analysis. *Marine Chemistry*, *157*, 170–184. https://doi.org/10.1016/j.marchem.2013.10.004

Lakowicz, J. R. (2006). *Principles of fluorescence spectroscopy*. Springer.

Lawaetz, A. J., & Stedmon, C. A. (2009). Fluorescence intensity calibration using the Raman scatter peak of water. *Applied Spectroscopy*, *63*(8), 936–940. https://doi.org/10.1366/000370209788964548

Liu, H., Zhou, H., Yang, W., Liu, X., Li, Y., Yang, Y., et al. (2021). A three-dimensional gravest empirical mode determined from hydrographic observations in the western equatorial Pacific Ocean. *Journal of Marine Systems*, *214*, 103487. https://doi.org/10.1016/j.jmarsys.2020.103487

Liu, Z. Y., Lian, Q., Zhang, F. T., Wang, L., Li, M. M., Bai, X. L., et al. (2017). Weak thermocline mixing in the North Pacific low-latitude western boundary current system. *Geophysical Research Letters*, *44*(20), 10530–10539. https://doi.org/10.1002/2017gl075210

Lønborg, C., Yokokawa, T., Herndl, G. J., & Alvarez-Salgado, X. A. (2015). Production and degradation of fluorescent dissolved organic matter in surface waters of the eastern North Atlantic Ocean. *Deep Sea Research Part I: Oceanographic Research Papers*, *96*, 28–37. https://doi.org/10.1016/j.dsr.2014.11.001

Martínez-Pérez, A. M., Catalá, T. S., Nieto-Cid, M., Otero, J., Alvarez, M., Emelianov, M., et al. (2019). Dissolved organic matter (DOM) in the open Mediterranean Sea. II: Basin-wide distribution and drivers of fluorescent DOM. *Progress in Oceanography*, *170*, 93–106. https://doi.org/10.1016/j.pocean.2018.10.019

Millard, R. C., Owens, W. B., & Fofonoff, N. P. (1990). On the calculation of the Brunt-Väisälä frequency. *Deep-Sea Research*, *37*, 167–181. https://doi.org/10.1016/0198-0149(90)90035-T

Mopper, K., Kieber, D. J., & Stubbins, A. (2015). Chapter 8. Marine photochemistry of organic matter. In D. A. Hansell, & C. A. Carlson (Eds.), *Biogeochemistry of marine dissolved organic matter* (2nd ed., pp. 389–450). Academic Press. https://doi.org/10.1016/b978-0-12-405940-5.00008-x

Moutin, T., & Prieur, L. (2012). Influence of anticyclonic eddies on the Biogeochemistry from the Oligotrophic to the Ultraoligotrophic Mediterranean (BOUM cruise). *Biogeosciences*, *9*(10), 3827–3855. https://doi.org/10.5194/bg-9-3827-2012

Nelson, N. B., Siegel, D. A., Carlson, C. A., & Swan, C. M. (2010). Tracing global biogeochemical cycles and meridional overturning circulation using chromophoric dissolved organic matter. *Geophysical Research Letters*, *37*. https://doi.org/10.1029/2009gl042325

Nieto-Cid, M., Álvarez-Salgado, X. A., & Pérez, F. F. (2006). Microbial and photochemical reactivity of fluorescent dissolved organic matter in a coastal upwelling system. *Limnology & Oceanography*, *51*(3), 1391–1400. https://doi.org/10.4319/lo.2006.51.3.1391

Ohno, T. (2002). Fluorescence inner-filtering correction for determining the humification index of dissolved organic matter. *Environmental Science & Technology*, *36*(4), 742–746. https://doi.org/10.1021/es0155276

Qiu, B., & Chen, S. C. (2010). Interannual-to-decadal variability in the bifurcation of the North Equatorial Current off the Philippines. *Journal of Physical Oceanography*, *40*(11), 2525–2538. https://doi.org/10.1175/2010jpo4462.1

Qiu, B., & Lukas, R. (1996). Seasonal and interannual variability of the North Equatorial Current, the Mindanao Current, and the Kuroshio along the Pacific western boundary. *Journal of Geophysical Research: Oceans*, *101*(C5), 12315–12330. https://doi.org/10.1029/95jc03204

Qu, L., Wu, Y., Li, Y., Stubbins, A., Dahlgren, R. A., Chen, N., & Guo, W. (2020). El Nino-driven dry season flushing enhances dissolved organic matter export from a subtropical watershed. *Geophysical Research Letters*, *47*(19). https://doi.org/10.1029/2020gl089877

Qu, T. D., Mitsudera, H., & Yamagata, T. (1998). On the western boundary currents in the Philippine Sea. *Journal of Geophysical Research: Oceans*, *103*(C4), 7537–7548. https://doi.org/10.1029/98jc00263

Qu, T. D., Mitsudera, H., & Yamagata, T. (1999). A climatology of the circulation and water mass distribution near the Philippine Coast. *Journal of Physical Oceanography*, *29*, 1488–1505. https://doi.org/10.1175/1520-0485(1999)029<1488:acotca>2.0.co;2

Raymond, P. A., & Spencer, R. G. M. (2015). Chapter 11—Riverine DOM. In D. A. Hansell, & C. A. Carlson (Eds.), *Biogeochemistry of marine dissolved organic matter* (2nd ed., pp. 509–533). Academic Press. https://doi.org/10.1016/B978-0-12-405940-5.00011-X

Rochelle-Newall, E. J., & Fisher, T. R. (2002). Production of chromophoric dissolved organic matter fluorescence in marine and estuarine environments: An investigation into the role of phytoplankton. *Marine Chemistry*, *77*(1), 7–21. https://doi.org/10.1016/s0304-4203(01)00072-x

Romera-Castillo, C., Sarmento, H., Alvarez-Salgado, X. A., Gasol, J. M., & Marrase, C. (2010). Production of chromophoric dissolved organic matter by marine phytoplankton. *Limnology & Oceanography*, *55*(1), 446–454. https://doi.org/10.4319/lo.2010.55.1.0446

Shen, Y., & Benner, R. (2019). Molecular properties are a primary control on the microbial utilization of dissolved organic matter in the ocean. *Limnology & Oceanography*, *65*, 1061–1071. https://doi.org/10.1002/lno.11369

Spencer, R. G. M., & Coble, P. (2014). Chapter 4—Sampling design for organic matter fluorescence analysis. In P. Coble, J. Lead, A. Baker, D. M. Reynolds, & R. G. M. Spencer (Eds.), *Aquatic organic matter fluorescence* (pp. 125–146). Cambridge University Press.

Ueki, I., Kashino, Y., & Kuroda, Y. (2003). Observation of current variations off the New Guinea coast including the 1997—1998 El Niño period and their relationship with Sverdrup transport. *Journal of Geophysical Research*, *108*(C7). https://doi.org/10.1029/2002jc001611

Wang, C., Guo, W. D., Li, Y., Stubbins, A., Li, Y. Z., Song, G. D., et al. (2017). Hydrological and biogeochemical controls on absorption and fluorescence of dissolved organic matter in the Northern South China Sea. *Journal of Geophysical Research: Biogeosciences*, *122*(12), 3405–3418. https://doi.org/10.1002/2017jg004100

Wang, C. Z. (2019). Three-ocean interactions and climate variability: A review and perspective. *Climate Dynamics*, *53*(7), 5119–5136. https://doi.org/10.1007/s00382-019-04930-x

Welschmeyer, N. A. (1994). Fluorometric analysis of chlorophyll a in the presence of chlorophyll b and pheopigments. *Limnology & Oceanography*, *39*, 1985–1992. https://doi.org/10.4319/lo.1994.39.8.1985

Wijffels, S. E., Meyers, G., & Godfrey, J. S. (2008). A 20-yr average of the Indonesian throughflow: Regional currents and the interbasin exchange. *Journal of Physical Oceanography*, *38*(9), 1965–1978. https://doi.org/10.1175/2008jpo3987.1

Wu, K., Dai, M. H., Chen, J. H., Meng, F. F., Li, X. L., Liu, Z. Y., et al. (2015). Dissolved organic carbon in the South China Sea and its exchange with the Western Pacific Ocean. *Deep Sea Research Part II: Topical Studies in Oceanography*, *122*, 41–51. https://doi.org/10.1016/j.dsr2.2015.06.013

Xu, M. N., Zhang, W., Zhu, Y., Liu, L., Zheng, Z., Wan, X. S., et al. (2018). Enhanced ammonia oxidation caused by lateral Kuroshio intrusion in the boundary zone of the northern South China Sea. *Geophysical Research Letters*, *45*(13), 6585–6593. https://doi.org/10.1029/2018gl077896

Yamashita, Y., Hashihama, F., Saito, H., Fukuda, H., & Ogawa, H. (2017). Factors controlling the geographical distribution of fluorescent dissolved organic matter in the surface waters of the Pacific Ocean. *Limnology & Oceanography*, *62*(6), 2360–2374. https://doi.org/10.1002/lno.10570

Zhou, H., Liu, H. C., Tan, S., Yang, W., Li, Y., Liu, X., et al. (2021). The observed North Equatorial Counter Current in the far western Pacific Ocean during the 2014–2016 El Niño. *Journal of Physical Oceanography*, *51*(6), 2003–2020. https://doi.org/10.1175/JPO-D-20-0293.1

Zhou, H., Yuan, D. L., Guo, P. F., Shi, M. C., & Zhang, Q. L. (2010). Mesoscale circulation at the intermediate-depth east of Mindanao observed by Argo profiling floats. *Science China Earth Sciences*, *53*(3), 432–440. https://doi.org/10.1007/s11430-009-0196-7

Zhou, K. B., Dai, M. H., Kao, S. J., Wang, L., Xiu, P., Chai, F., et al. (2013). Apparent enhancement of Th-234-based particle export associated with anticyclonic eddies. *Earth and Planetary Science Letters*, *381*, 198–209. https://doi.org/10.1016/j.epsl.2013.07.039